ACS OMEGA

http://pubs.acs.org/journal/acsodf

Article

Sensitive Determination of SARS-COV-2 and the Anti-hepatitis C Virus Agent Velpatasvir Enabled by Novel Metal−Organic Frameworks

Mahmoud A. Saleh, Mona A. Mohamed, Ahmed Shahat, and Nageh K. Allam*

Cite This: *ACS Omega* 2021, 6, 26791−26798

Read Online

ACCESS | Metrics & More | Article Recommendations | Supporting Information

ABSTRACT: Herein, we report on the electrochemical determination of velpatasvir (VLP) as the main constituent of Epclusa, a SARS-COV-2 and anti-hepatitis C virus (HCV) agent, using a novel metal−organic framework (MOF). The NH_2-MIL-53(Al) MOF was successfully modified with 5-bromo-salicylaldehyde to synthesize 5-BSA=N-MIL-53(Al) MOF. The synthesized MOF has been characterized using Fourier transform infrared spectroscopy, X-ray powder diffraction, scanning electron microscopy, cyclic voltammetry, square wave voltammetry, and electrochemical impedance spectroscopy. The modified MOF showed higher electrochemical activity and response than the bare NH_2-MIL-53(Al) MOF. Compared to the bare carbon paste electrode (CPE), the 5-BSA=N-MIL-53(Al)/CPE platform was shown to enhance the electrochemical oxidation and detection of the anti-SARS-COV-2 and anti-HCV agent. Under optimized conditions, the 5-BSA=N-MIL-53(Al)/CPE platform showed a linear range of 1.11×10^{-6} to 1.11×10^{-7} and 1.11×10^{-7} to 25.97×10^{-6} M Britton−Robinson buffer (pH 7) with a detection limit and limit of quantification of 8.776×10^{-9} and 2.924×10^{-8} M, respectively. Repeatability, storage stability, and reproducibility in addition to selectivity studies and interference studies were conducted to illustrate the superiority of the electrode material. The study also included a highly accurate platform for the determination of VLP concentrations in both urine and plasma samples with reasonable recovery.

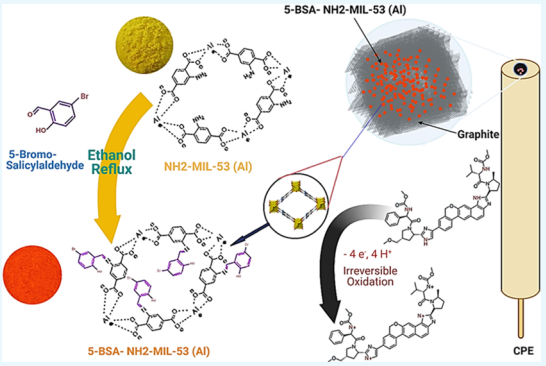

1. INTRODUCTION

Velpatasvir (VLP) is a direct-acting NS5A inhibitor, a generic product Epclusa in combination with sofosbuvir, that is used for the pan-genotypic treatment of chronic hepatitis C viral (HCV) infection.[1−4] In addition, Epclusa was found to possess a high potential of SARS-COV-2 inhibition.[5−11] HCV is a ribonucleic acid virus discovered in 1989, which is the most common predisposing factor for chronic liver disease, liver cirrhosis, and liver cancer in addition to liver transplant surgery in the US and many other countries around the world.[12−15] In 2016, Epclusa—VLP in combination with sofosbuvir (a single 12 week regimen tablet for all HCV genotypes)—was proposed as a revolutionary treatment of HCV complicated and non-complicated patients.[2,16] This makes the greatest turnover in this century in HCV prognosis, providing the best sustained viral response among other combinations of direct-acting antiviral agents (DAAAs) by achieving 99% sustained viral response decompensated cirrhotic patients in a 12 week regimen.[2,16] On the other hand, using molecular docking analyses,[9] Epclusa has shown to exhibit high efficiency against COVID-19.[6,7] This was ascribed to the similarity between nonstructural protein 12 (nsp12) in both HCV and SARS-COV-2 RNA polymerases, which was found to possess high potential for SARS-COV-2 viral infection.[6,7]

The necessity to monitor such a life-saving drug emerges from the fact that it is extensively metabolized by liver cytochrome P450 enzymes; CYP2B6, CYP2C8, and CYP3A4.[17,18] This makes its metabolism prone to alteration by other inhibiting therapeutic agents that affect those enzymes. To this end, VLP determination in the presence of sofosbuvir was reported using a plethora of methods, including LC−MS/MS,[19,20] UPLC-ESCI MS/MS,[21] HPLC−MS/MS,[22] and HPTLC,[23] in biological fluids and clinical studies. In addition, the determination of the two drugs in their pharmaceutical formula was addressed utilizing UPLC,[24] spectrofluorimetry,[25] UPLC/spectrofluorimetry,[26] and spectrophotometry.[27] However, the determination range is somewhat expensive and time-consuming. In this regard, electrochemistry can provide highly sensitive and rapid analysis techniques that are simple and cost-effective.[28−33] The electrochemical determination of VLP using the molecular-

Received: August 19, 2021
Accepted: September 17, 2021
Published: September 30, 2021

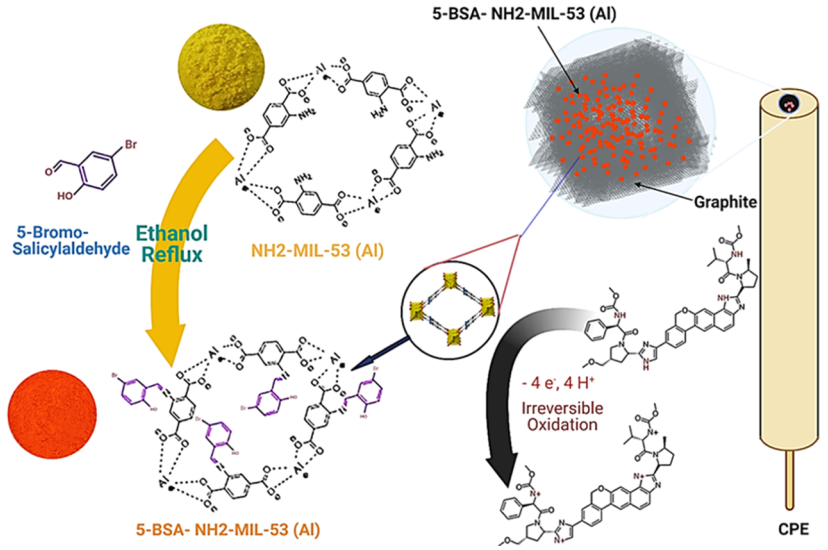

Figure 1. Schematic of the preparation of 5-BSA=N-MIL-53(Al) and the suggested oxidation mechanism of VLP.

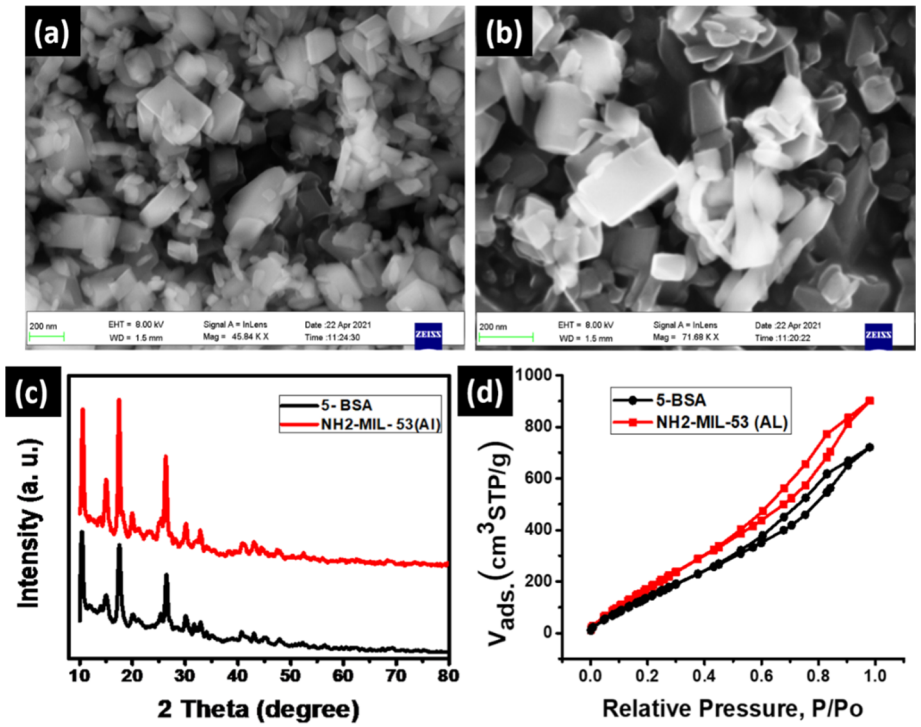

Figure 2. FESEM images of (a) NH_2-MIL-53 (Al) and (b) 5-BSA=N-MIL-53(Al), (c) XRD of both NH_2-MIL-53(Al) and 5-BSA=N-MIL-53(Al), and (d) BET adsorption−desorption isotherms of NH_2-MIL-53(Al) and 5-BSA=N-MIL-53(Al).

imprinted polymer deposited on a 3D starfish-like hollow nickel skeleton decorated with the MWCNT−Au NP-modified glassy carbon electrode has recently been reported in pharmaceutical formula and biological fluids.[34] Despite the achieved good linearity (5.66−90.60 nM) and low limit of detection (LOD) (0.227 nM), the high cost of the composite and the tedious synthesis method render the whole process hard to adopt for routine analysis.[34] These limitations necessitate the search for alternative platforms.

Herein, we demonstrate the use of 5-bromo-salicylaldehyde-NH_2-MIL-53(Al) (5-BSA) as an efficient and novel metal−organic framework (MOF) material with superior electrochemical properties. Note that NH_2-MIL-53(Al) was shown to be efficient in the detection of mercury ions in water with a low detection limit.[35,36] Our modification of NH_2-MIL-53(Al) yielded a much more highly responsive MOF with superior conductivity. Specifically, the fabricated 5-BSA=N-MIL-53(Al) was investigated as a sensor material for the electrochemical determination of VLP, knowing that sofosbuvir is electrochemically inactive,[37,38] in buffer solutions and biological fluids. Our proposed platform presents a cheap, feasible, and convenient method of preparing a sensor with the wide range of linearity (0.11−25.97 μM), while providing a comparable LOD of 8.776 nM.

https://doi.org/10.1021/acsomega.1c04525
ACS Omega 2021, 6, 26791−26798

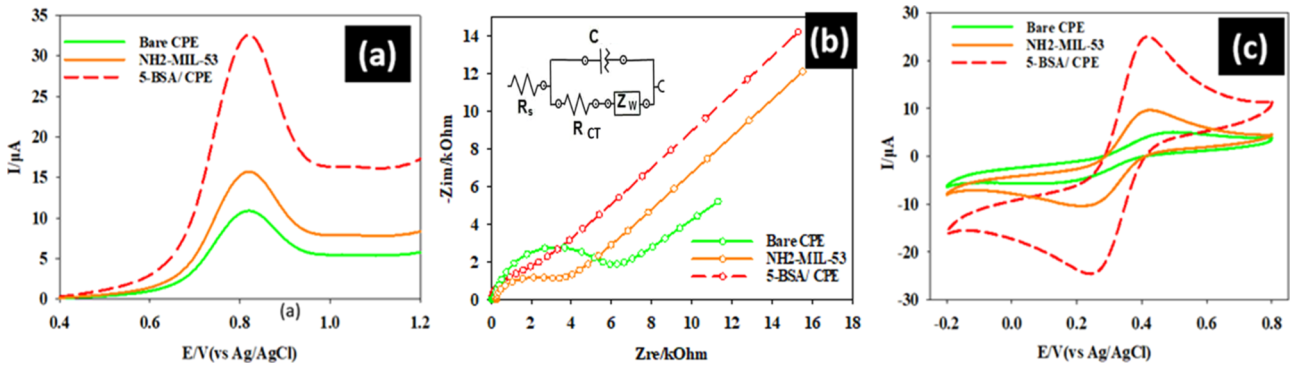

Figure 3. (a) Square wave voltammograms (SWV) of 0.1 mM of VLP in BRB (pH 7.0) at a scan rate of 0.1 V s^{-1}, (b) impedance plots at a scan rate of 0.1 V s^{-1} in 1.0 mM $K_3Fe(CN)_6$ in 0.1 M KCl, and (c) CVs of 1.0 mM $K_3Fe(CN)_6$ in 0.1 M KCl at a scan rate of 100 mV·s^{-1}.

RESULTS AND DISCUSSION

Surface Characterization of the Fabricated Sensor. The surface amine groups are sacrificed to modify the surface of the parent MOF via the reaction of the 5-bromosalicylaldehyde ligand with the amino groups, resulting in the formation of the salicylidene [R−N═C−C_6H_4OH(Br)] moiety as a bidentate ligand, Figure 1.

Figure 2a,b depicts the field emission scanning electron microscopy (FESEM) images of NH_2-MIL-53(Al) and 5-BSA=N-MIL-53(Al), respectively. The images reveal sheet-like structures with a mean side length of ∼118 ± 2 nm. Note that the addition of 5-bromosalicylaldehyde does not result in a profound change in the morphology of the material. To elucidate the crystal structure and phase purity of the NH_2-MIL-53(Al) MOF and 5-BSA=N-MIL-53(Al) materials, X-ray diffraction (XRD) spectra are recorded, as depicted in Figure 2c. The XRD spectra of both NH_2-MIL-53(Al) and 5-BSA=N-MIL-53(Al) indicate similar peaks at 2θ = 8.8, 10.5, 15.08, 17.5, 20.2, and 26.4°.[39−41] Hence, 5-BSA=N-MIL-53(Al) and NH_2-MIL-53(Al) possess the same crystalline structure with no change upon imine formation. However, the broadness of the XRD peaks of NH_2-MIL-53(Al) reveals a smaller crystallite size.[47]

The BET adsorption isotherm of NH_2-MIL-53(Al), as depicted in Figure 2d, reveals type IV isotherm. The steep increase upon increasing the relative pressure in the low-pressure region indicates a microporous structure,[42,43] while the hysteresis loop in the high-pressure region reveals mesoporous characteristics.[44,45] The BET surface area of NH_2-MIL-53(Al) is estimated to be 794 $m^2 \cdot g^{-1}$, which is decreased to 652 $m^2 \cdot g^{-1}$ for the 5-BSA=N-MIL-53(Al) counterpart, revealing the preservation of free $-NH_2$ within the NH_2-MIL-53(Al). The non-local density functional theory method is used to determine the cumulative pore volume of 5-BSA=N-MIL-53(Al) and NH_2-MIL-53(Al). Comparatively, the pore volume of the prepared 5-BSA=N-MIL-53(Al) (1.111 cm^3/g) is found to be lower than the parent NH_2-MIL-53(Al) MOF (1.407 cm^3/g). This decrease in both the surface area and pore volume is indicative of the successful post-synthetic imine formation. The pore radii, as estimated from the BJH model, for 5-BSA=N-MIL-53(Al) and NH_2-MIL-53(Al) were found to be 1.89 and 1.99 nm, respectively. Therefore, the micropore diameters of the 5-BSA=N-MIL-53(Al) and NH_2-MIL-53(Al) seem to be distributed within this range. The Fourier transform infrared spectroscopy (FTIR) spectra (Figure S1) of both 5-BSA=N-MIL-53(Al) and NH_2-MIL-53(Al) reveal $-NH_2$ symmetric and asymmetric stretches of the NH_2-BDC (benzene dicarboxylic) ligand at 3492 and 3384 cm^{-1}.[46] However, the peaks at 3501 and 3384 cm^{-1} assigned to the N−H were diminished in the case of 5-BSA=N-MIL-53(Al), indicating the formation of the imine group upon the reaction of the amine of the NH_2-BDC ligand with the aldehyde group of the 5-formylsalicylaldehyde ligand.[46,47]

Electrochemical Characterization. The square wave voltammetry (SWV) technique is utilized to elucidate the electrochemical performance of the bare carbon paste electrode (CPE) compared to the 5-BSA=N-MIL-53(Al)-modified CPE for the electrochemical oxidation of VLP in Britton−Robinson buffer (BRB) (pH 7.0) using 1.0 × 10^{-3} M VLP, Figure 3a. Neither anodic nor cathodic beaks are detected in the absence of VLP, which demonstrates that our sensor platform has no electrochemical activity in the working potential window. For the unmodified CPE, the I_p of the electrochemical oxidation of VLP is 14.03 μA at 8820 mV, which is greatly increased to 36.12 μA at 8226 mV upon the modification of the bare CPE with 5-BSA. This enhancement in I_p reveals the facile oxidation of VLP on the modified electrode, revealing the necessity of using 5-BSA=N-MIL-53(Al) for the sensitive lower potential detection of VLP.

The electrochemically active surface area of the 5-BSA=N-MIL-53(Al)-modified CPE was estimated from the cyclic voltammogram (CV) using the Randles−Ševčík equation (eq 1). For a quasi-reversible reaction in a 1:1 solution of 1.0 × 10^{-3} M $K_3Fe(CN)_6$ and 0.10 M KCl, recording the current is elucidated versus peak potential at various scan rates.[48]

$$I_p = 2.65 \times 10^5 n^{3/2} A D^{1/2} C \nu^{1/2} \quad (1)$$

where I_p is the peak current, n is the number of electrons involved in the electrochemical anodic oxidation, D is the diffusion coefficient, C is the redox probe concentration, A is the electrochemical surface area of the electrode, and ν is the applied scan rate. The D for $K_3Fe(CN)_6$ was taken as 7.6 × 10^{-6} cm^2 s^{-1}.[48] The electrochemically active surface areas of the bare CPE and the 5-BSA=N-MIL-53(Al)-modified CPE were 0.067 and 0.338 cm^2, as calculated from the slopes of the I_p versus $\nu^{1/2}$ graphs.

Utilizing the electrochemical impedance spectroscopy (EIS) diagrams (Figure 3b), reaction kinetics, mass transport, and charge-transfer coefficient through the electrode surface were inspected using a 1:1 solution of 1.0 × 10^{-3} M $K_3Fe(CN)_6$ in 0.1 M KCl. Note the quasi-circle in the high-frequency window, where the diameter of the semi-circle enables the

https://doi.org/10.1021/acsomega.1c04525
ACS Omega 2021, 6, 26791−26798

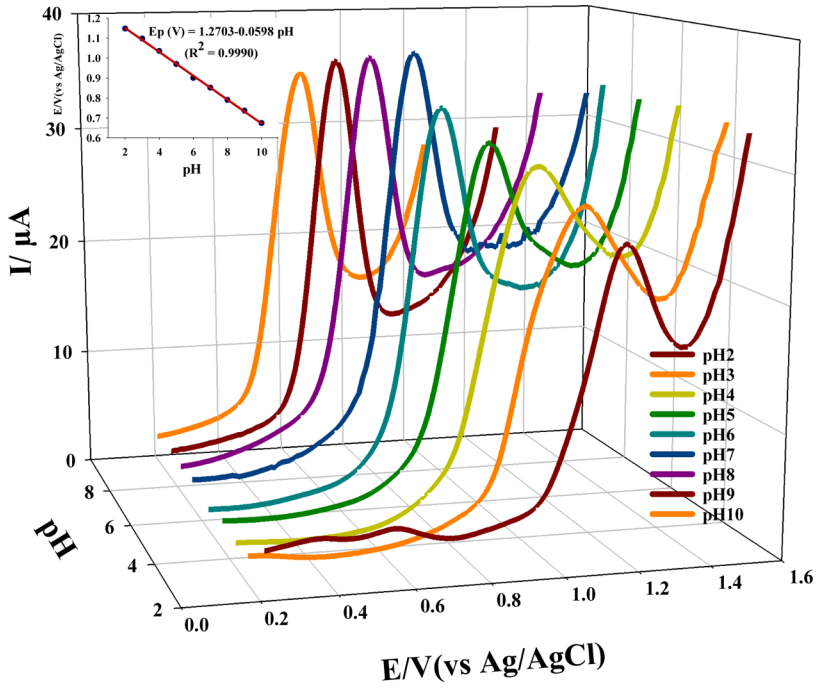

Figure 4. SWV of 0.1 mM of VLP at different pH values of BRB using 5-BSA=N-MIL-53(Al) at a scan rate of 0.1 V s^{-1}. The inset linear graph shows the linear relationship between the solution pH and the peak potential (E_p).

estimation of the charge-transfer resistance at the electrode/electrolyte interface (R_{CT}). The Nyquist plot reveals a Warburg-type equivalent circuit model. Thus, modifying the CPE with the proposed MOF enhances the charge transfer compared to the unmodified CPE. Upon fitting, the R_{CT} of the bare CPE is found to be 4400 Ω that sharply decreases to 1541.13 Ω upon modification with 5-BSA=N-MIL-53(Al), which can be attributed to the large surface area of the MOF and its interactive nature that enhances electron transfer. Moreover, the electrochemical activity of the bare CPE is compared to that of the 5-BSA=N-MIL-53(Al)/CPE electrode in a 1:1 solution of 1.0×10^{-3} M $K_3Fe(CN)_6$ in 0.1 M KCl, as illustrated in Figure 3c. The anodic peak current value of the 5-BSA=N-MIL-53(Al)/CPE electrode is almost five times than that of the bare CPE. Furthermore, the use of the 5-BSA=N-MIL-53(Al)/CPE decreased the peak separation ($E_{p\ anodic} - E_{p\ cathodic}$) significantly from 0.32 to 0.17 V in comparison to the bare CPE, revealing enhanced electron transfer.[30] Therefore, 5-BSA=N-MIL-53(Al) has a good catalytic activity toward the electrochemical oxidation of VLP, good conductivity, and a high rate of electron transfer.

Effect of pH. The effect of pH on the electrochemical anodic oxidation of VLP is assessed in the pH range of 2.0−10.0, as shown in Figure 4. Upon varying the pH of the solution from 2 to 10, the peak potential shifts toward the zero potential, indicating the protonation−deprotonation electrochemical reaction of VLP.[49] Plotting the peak potential (E_p) versus the buffered solution pH, the voltammetric response of VLP can be assessed as E_p (V) = 1.2703−0.0598 pH (R^2 = 0.9990). It is found that the slope of the obtained linear relationship is near to the known Nernstian value of a one electron−one proton electrochemical oxidative reaction, as indicated in Figure 4, which is 59.0 mV per pH unit at ambient temperature. Utilizing the Nernstian behavior of VLP electrochemical oxidation, the suggested mechanism of oxidation is depicted in Figure 1.

Effect of the Scan Rate. The effect of the scan rate on the electrochemical anodic oxidation of VLP is investigated using the 5-BSA=N-MIL-53(Al)/CPE and CV, Figure 5. Upon

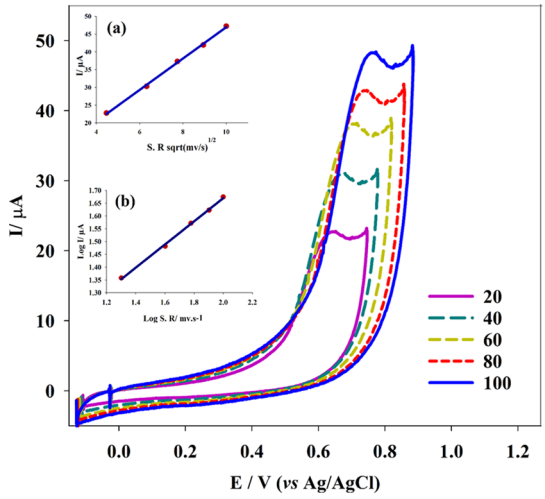

Figure 5. CV of 0.10 mM VLP at pH 7.0 using the 5-BSA=N-MIL-53(Al)/CPE in the wide scan rate (0.010−0.200 V s^{-1}). Insets: (a) plot of peak current vs the square root of the scan rate, and (b) plot of the algorithm of peak current vs the algorithm of the scan rate.

increasing the scan rate, the peak potential (E_p) is shifted into more positive values, indicating an irreversible electrochemical behavior of VLP. A linear relationship is obtained by plotting the peak current (I_p) versus the square root of the scan rate ($\nu^{1/2}$) in the range of 0.010−0.100 V s^{-1}. This indicates a diffusion-controlled process, as in equation I_p (µA) = 4.4194 $\nu^{1/2}$ (mV s^{-1}) + 2.7671 µA, R^2 = 0.9986, as illustrated in Figure 5(a). Furthermore, the slope of the relation between the algorithm of the scan rate and the measured current is less than 0.5, log I_p (µA) = 0.4529 mV s^{-1} + 0.7638 µA, R^2 = 0.9981,

https://doi.org/10.1021/acsomega.1c04525
ACS Omega 2021, 6, 26791−26798

which supports the point that the anodic oxidation process is diffusion-controlled one, as shown in Figure 5(b) All of these findings necessitate the use of the CPE modified with 5-BSA=N-MIL-53(Al).

Analytical Performance Validation. The proposed sensing protocol is optimized based on the accredited system of the International Conference on Harmonization.[50] SWV scans using the 5-BSA=N-MIL-53(Al)/CPE in BRB of pH 7.0 containing several dilutions of VLP were performed and analyzed. To achieve linearity, accuracy, and precision, the calibration curve is established taking into consideration the practical range of VLP in the normal tablet concentration. The SWVs of these dilutions are shown in Figure 6. At a scan rate

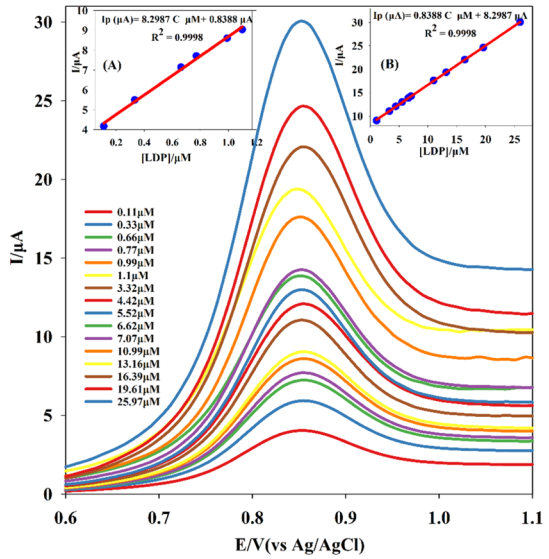

Figure 6. SWV of several dilutions of VLP (25.97−0.11 μM) in pH 7.0 BRB utilizing the 5-BSA=N-MIL-53(Al)/CPE sensor at a scan rate of 0.1 V s^{-1}. The inset illustrates the plot of the peak current as a function of concentrations in the range of 1.11×10^{-6} to 1.11×10^{-7} and 1.11×10^{-7} to 25.97×10^{-6} M.

of 0.1 V s^{-1}, VLP shows two linear behaviors based on its concentration in BRB. In the range of 1.11×10^{-7} to 1.11×10^{-6} M, the regression equation is I_p (μA) = 4.9059 C μM + 3.7830 μA, R^2 = 0.9954, while in the range of 1.11×10^{-6} to 25.97×10^{-6} M, the regression equation is I_p (μA) = 0.8388 C μM + 8.2987 μA, R^2 = 0.9954. The main cause for the decrease in the slope of the second linear range at higher concentrations is the increase in the required energy for anodic stripping in addition to the Ohmic drop at such high levels of VLP.[51] Furthermore, the LOD and limit of quantification (LOQ) are calculated to be 8.776×10^{-9} and 2.924×10^{-8} M, respectively.

$$\mathrm{LOD} = \frac{3\mathrm{SD}}{x} \tag{2}$$

$$\mathrm{LOQ} = \frac{10\mathrm{SD}}{x} \tag{3}$$

where SD is the standard deviation of I_p of VLP anodic oxidation for five trials and x is the slope of the calibration curve.

Repeatability, Storage Stability, and Reproducibility Studies. A sensor platform should possess three important characteristics, repeatability, storage stability, and reproducibility. Repeatability is tested by using the same electrode for 10 consecutive SWV scans against 0.10 mM VLP in pH 7.0 BRB and the relative standard deviation (RSD) was found to be 2.47%, as shown in Figure S2a. Stability analysis is evaluated by storing the electrode at ambient temperature after scanning it in similar conditions and repeating the SWV scanning every week for 4 weeks as illustrated in Figure S2b. Reproducibility is examined by plotting the I_p for 7 CVs of different freshly prepared electrodes, as shown in Figure S2c, where the RSD was found to be 1.21%.

Biological Sample Analysis. Utilizing the serial dilution method, vast concentrations of VLP in spiked plasma and urine samples have been determined electrochemically and compared to the added concentration in Table 1. The proposed 5-BSA=N-MIL-53(Al)/CPE sensor reveals a good precision via the recovery results, which showed no apparent changes from the added values. According to the electrochemical studies, the sensor can determine VLP concentrations in plasma and urine samples, as shown in Figure 7.

Table 1. Application of SWV for the Determination of VLP in Plasma and Urine Samples

sample	standard amount added (M)	amount found (M)	apparent recovery %
plasma	1.11×10^{-7}	$1.08 \times 10^{-7} \pm 0.09$	102.78
	7.77×10^{-7}	$7.88 \times 10^{-7} \pm 0.08$	101.53
	1.11×10^{-6}	$1.13 \times 10^{-6} \pm 0.04$	98.23
	7.07×10^{-6}	$7.09 \times 10^{-6} \pm 0.08$	99.71
	16.40×10^{-6}	$16.37 \times 10^{-6} \pm 0.06$	100.18
	25.97×10^{-6}	$26.02 \times 10^{-6} \pm 0.10$	100.20
Urine	1.11×10^{-7}	$1.12 \times 10^{-7} \pm 0.07$	99.10
	7.77×10^{-7}	$7.68 \times 10^{-7} \pm 0.05$	98.87
	1.11×10^{-6}	$1.07 \times 10^{-6} \pm 0.09$	103.73
	7.07×10^{-6}	$7.12 \times 10^{-6} \pm 0.04$	99.29
	16.40×10^{-6}	$16.44 \times 10^{-6} \pm 0.10$	99.75
	25.97×10^{-6}	$26.10 \times 10^{-6} \pm 0.07$	100.05

Interference Studies. The selectivity of the proposed 5-BSA=N-MIL-53(Al)/CPE sensor is determined in the presence of ascorbic acid as one of the prevalent elements in the plasma that can interfere with the electrochemical determination of some therapeutic elements.[52] The utilized 5-BSA=N-MIL-53(Al)/CPE sensor shows the ability to determine both ascorbic acid and VLP in the same pH 7.0 BRB solution as two separate peaks at 0.35 and 0.85 V, respectively, as shown in Figure S3. Other excipients that are commonly used during tablet manufacturing and can interfere with VLP determination have been determined electrochemically in the presence of 1.0 mM of VLP at pH 7.0 BRB solution separately, as shown in Figure S4. Note that none of the tested materials obviously interfered with the detection of VLP in solution with a tolerance limit of less than ±5.0% for each separate excipient. Therefore, we report a cheap and simple method for the electrochemical determination of VLP.

CONCLUSIONS

In conclusion, we report a novel method for the preparation of 5-BSA=N-MIL-53(Al) MOF as a platform for the electrochemical determination of VLP utilizing the CPE. The proposed method shows an accurate, stable, and reproductive means of detection. It also enables the determination of VLP in BRB, urine, and plasma. Compared to previous studies, the 5-

https://doi.org/10.1021/acsomega.1c04525
ACS Omega 2021, 6, 26791−26798

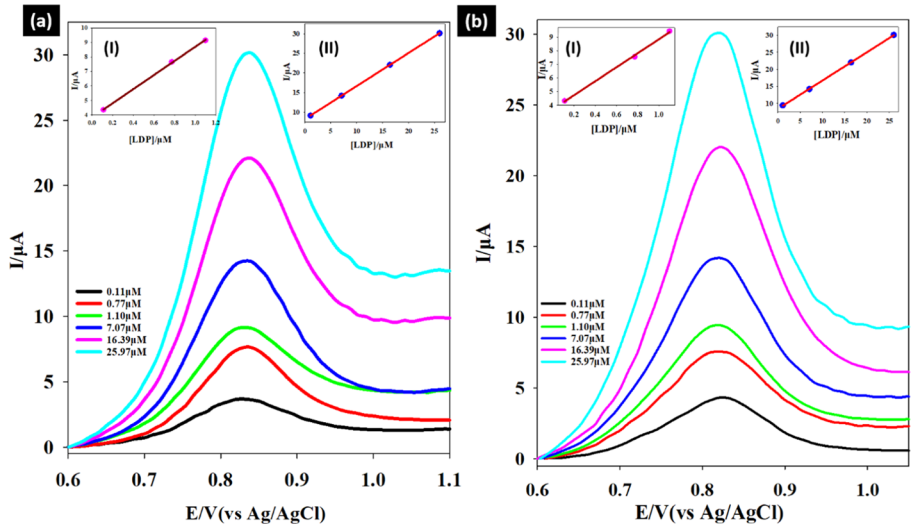

Figure 7. SWV for serial dilutions of VLP spiked (a) plasma samples and (b) urine samples 25.97−0.11 μM in pH 7.0 BRB utilizing the 5-BSA=N-MIL-53(Al)/CPE sensor at a scan rate of 0.1 V s^{-1}. Insets illustrate the plot of the peak current as a function of concentrations in the range of 1.11 × 10^{-6} to 1.11 × 10^{-7} and 1.11 × 10^{-7} to 25.97 × 10^{-6} M.

BSA=N-MIL-53(Al)/CPE sensor platform illustrates a simpler and cheaper alternative with a novel and easier method of preparation. The proposed method showed a comparable LOD and LOQ to previous studies with linearity of 1.11 × 10^{-6} to 1.11 × 10^{-7} and 1.11 × 10^{-7} to 25.97 × 10^{-6} M and LOD and LOQ of 8.776 × 10^{-9} and 2.924 × 10^{-8} M, respectively, in pH 7.0 BRB. Thus, the prepared sensor platform can show high competitiveness in the large-scale production of VLP sensors.

EXPERIMENTAL SECTION

Materials and Reagents. 2-Aminoterephthalic acid (99.0%, Sigma-Aldrich), sodium hydroxide, NaOH (99.9%, Alfa Aesar), $AlCl_3·6H_2O$ (99.0%, Sigma-Aldrich), salicylaldehyde (98.0%, Sigma-Aldrich), acetic acid (≥99%, Sigma-Aldrich), bromine (≥99.99%, Sigma-Aldrich), and ethanol (99.5%, Sigma-Aldrich) were used. All chemicals and reagents were used as received without any purification.

Apparatus. The electrochemical properties of the samples were analyzed using a Bio-Logic 300 electrochemical workstation. A platinum wire electrode (BAS, USA) was used as the counter electrode, and a Ag/AgCl (BAS, USA, 3.0 M NaCl) was used as the reference electrode. A Hanna HI-5522 pH meter (Hanna instruments, USA) was used to measure the pH. All electrochemical experiments were conducted at an ambient temperature of 25 °C. The EIS measurements were conducted in the frequency range of 100 mHz−100 kHz. Scanning electron microscopy (SEM) imaging was performed using a JSM-6700F scanning electron microscope (Japan Electro Company). FTIR spectra were recorded using an IR-Affinity-1 Fourier transform infrared spectrophotometer (Shimadzu, Japan). The XRD spectra and crystalline phases were determined using an X-ray diffractometer on an X'Pert Pro MRD with a copper source at a scan rate (2θ) of 1° s^{-1}. Sigma Plot 14.0 was used for all statistical data.

Sensor Fabrication. The CPE was prepared by mixing 1.0 g of graphite powder and 0.27 mL of paraffin oil uniformly by grinding in a small mortar. Then, a small amount of the paste is packed into the cavity of the electrode. The surface of the CPE is smoothed by polishing on a clean paper before its use. The CPE was immersed in the supporting electrolyte prior to scanning. After each scan, the paste is emptied, regenerated, and polished. The modified electrode was prepared by mixing 940 mg of graphite with 60 mg of 5-BSA, and the mixture is homogenized by mixing with a spatula and pestle for 45 min. Furthermore, 0.27 mL of paraffin was added and mixed to obtain the paste. The paste is packed and regenerated as aforementioned. Further addition of α-MnO_2−V_2O_5 to the graphite powder (more than 60 mg) did not make any difference in the I_p.

Sensor Testing. *Analysis of Plasma Samples.* Fresh plasma samples were collected from a healthy individual before the experiments. 10 μL of the supernatant was added to 4.5 mL of pH 7 BRB with different volumes of VLP stock solution in order to reach the desired concentration. The solution was transferred to an electrochemical cell for analysis without any further pretreatment, as described in Figure 7.

Analysis of Urine Samples. Fresh urine samples were collected from a healthy individual before the experiments. 10 μL of the supernatant was added to 4.5 mL of pH 7 BRB with different volumes of VLP stock solution in order to reach the desired concentration. The solution was transferred to an electrochemical cell for analysis without any further pretreatment, as described in Figure 7.

ASSOCIATED CONTENT

Supporting Information

The Supporting Information is available free of charge at https://pubs.acs.org/doi/10.1021/acsomega.1c04525.

FTIR spectra of the synthesized MOF, detailed procedure for the synthesis of 5-BSA=N-MIL-53(Al), standard and working solutions, recommended experimental procedures, SWV of a mixture of 10 μM VLP and ascorbic acid, response peak current (I_p) of the 5-BSA/CPE of 0.10 mM VLP, and obtained I_p of SWV of a 0.10 mM VLP mixture with the most used excipients at pH 7.0 using the 5-BSA=N-MIL-53(Al)/CPE (PDF)

https://doi.org/10.1021/acsomega.1c04525
ACS Omega 2021, 6, 26791−26798

AUTHOR INFORMATION

Corresponding Author

Nageh K. Allam − *Energy Materials Laboratory, Department of Physics, School of Sciences and Engineering, The American University in Cairo, New Cairo 11835, Egypt*; orcid.org/0000-0001-9458-3507; Email: nageh.allam@aucegypt.edu

Authors

Mahmoud A. Saleh − *Energy Materials Laboratory, Department of Physics, School of Sciences and Engineering, The American University in Cairo, New Cairo 11835, Egypt*

Mona A. Mohamed − *Energy Materials Laboratory, Department of Physics, School of Sciences and Engineering, The American University in Cairo, New Cairo 11835, Egypt*

Ahmed Shahat − *Chemistry Department, Faculty of Science, Suez University, Suez 43518, Egypt*; orcid.org/0000-0001-9198-9712

Complete contact information is available at: https://pubs.acs.org/10.1021/acsomega.1c04525

Notes

The authors declare no competing financial interest.

ACKNOWLEDGMENTS

The partial support of this work by the American University in Cairo is highly appreciated.

REFERENCES

(1) Chahine, E. B.; Sucher, A. J.; Hemstreet, B. A. Sofosbuvir/Velpatasvir: The First Pangenotypic Direct-Acting Antiviral Combination for Hepatitis C. *Annals of Pharmacotherapy*; SAGE Publications Inc., 2017; Vol. *51*, pp 44−53.

(2) Feld, J. J.; Jacobson, I. M.; Hézode, C.; Asselah, T.; Ruane, P. J.; Gruener, N.; Abergel, A.; Mangia, A.; Lai, C.-L.; Chan, H. L. Y.; et al. Sofosbuvir and Velpatasvir for Hcv Genotype 1, 2, 4, 5, and 6 Infection. *N. Engl. J. Med.* **2015**, *373*, 2599−2607.

(3) Gayam, V.; Gill, A.; Garlapati, P.; Mohanty, S. Direct-Acting Antivirals in Chronic Hepatitis C Infection with Liver Cirrhosis. *Hepatitis B and C*; IntechOpen, 2020.

(4) Zhuang, L.; Li, J.; Zhang, Y.; Ji, S.; Li, Y.; Zhao, Y.; Li, B.; Li, W.; Quan, M.; Duan, Y.; et al. Real-World Effectiveness of Direct-Acting Antiviral Regimens against Hepatitis C Virus (HCV) Genotype 3 Infection: A Systematic Review and Meta-Analysis. *Ann. Hepatol.* **2021**, *23*, 100268.

(5) Izzi, A.; Messina, V.; Rinaldi, L.; Maggi, P. Editorial - Sofosbuvir/Velpatasvir as a Combination with Strong Potential Activity against SARS-CoV2 (COVID-19) Infection: How to Use Direct-Acting Antivirals as Broad-Spectrum Antiviral Agents. *Eur. Rev. Med. Pharmacol. Sci.* **2020**, *24*, 5193−5194.

(6) Kumar, P.; Kulkarni, A.; Sharma, M.; Rao, P. N. Repurposing Hepatitis C Direct-Acting Antivirals Against COVID-19. *J. Clin. Exp. Hepatol.*; Elsevier B.V, 2021, *11*. 273-275DOI: DOI: 10.1016/j.jceh.2020.10.001.

(7) Gao, Y.; Yan, L.; Huang, Y.; Liu, F.; Zhao, Y.; Cao, L.; Wang, T.; Sun, Q.; Ming, Z.; Zhang, L.; et al. Structure of the RNA-Dependent RNA Polymerase from COVID-19 Virus. *Science* **2020**, *368*, 779−782.

(8) Jockusch, S.; Tao, C.; Li, X.; Chien, M.; Kumar, S.; Morozova, I.; Kalachikov, S.; Russo, J. J.; Ju, J. Sofosbuvir Terminated RNA Is More Resistant to SARS-CoV-2 Proofreader than RNA Terminated by Remdesivir. *Sci. Rep.* **2020**, *10*, 16577.

(9) Elfiky, A. A. Anti-HCV, Nucleotide Inhibitors, Repurposing against COVID-19. *Life Sci.* **2020**, *248*, 117477.

(10) Ju, J.; Kumar, S.; Li, X.; Jockusch, S.; Russo, J. J. Nucleotide Analogues as Inhibitors of Viral Polymerases. **2020**, bioRxiv:2020.01.30.927574. DOI: 10.1101/2020.01.30.927574.

(11) Liu, S.; Lien, C. Z.; Selvaraj, P.; Wang, T. T. Evaluation of 19 Antiviral Drugs against SARS-CoV-2 Infection. **2020**, bioRxiv:2020.04.29.067983.

(12) Khullar, V.; Firpi, R. J. Hepatitis C Cirrhosis: New Perspectives for Diagnosis and Treatment. *World J. Hepatol.* **2015**, *7*, 1843−1855.

(13) Alter, M. J. The Epidemiology of Acute and Chronic Hepatitis C. *Clin. Liver Dis.* **1997**, *1*, 559−568.

(14) Wasley, A.; Alter, M. J. Epidemiology of Hepatitis C: Geographic Differences and Temporal Trends. *Semin. Liver Dis.* **2000**, *20*, 1−16.

(15) Chen, S. L.; Morgan, T. R. The Natural History of Hepatitis C Virus (HCV) Infection. *Int. J. Med. Sci.* **2006**, *1*, 47−52.

(16) Inc, G. S. US Food and Drug Administration approves Gilead's Epclusa (sofosbuvir/velpatasvir) for treatment of all genotypes of chronic hepatitis C. https://www.gilead.com/news-and-press/press-room/press-releases/2016/6/us-food-and-drug-administration-approves-gileads-epclusa-sofosbuvirvelpatasvir-for-the-treatment-of-all-genotypes-of-chronic-hepatitis-c (accessed Jan 8, 2020).

(17) Greig, S. L. Sofosbuvir/Velpatasvir: A Review in Chronic Hepatitis C. *Drugs* **2016**, *76*, 1567−1578.

(18) Mogalian, E.; German, P.; Kearney, B. P.; Yang, C. Y.; Brainard, D.; Link, J.; McNally, J.; Han, L.; Ling, J.; Mathias, A. Preclinical Pharmacokinetics and First-in-Human Pharmacokinetics, Safety, and Tolerability of Velpatasvir, a Pangenotypic Hepatitis C Virus NS5A Inhibitor, in Healthy Subjects. *Antimicrob. Agents Chemother.* **2017**, *61*, No. e02084.

(19) Abdallah, O. M.; Abdel-Megied, A. M.; Gouda, A. S. Development and Validation of LC-MS/MS Method for Simultaneous Determination of Sofosbuvir and Daclatasvir in Human Plasma: Application to Pharmacokinetic Study. *Biomed. Chromatogr.* **2018**, *32*, No. e4186.

(20) Elkady, E. F.; Aboelwafa, A. A. Rapid Bioanalytical LC-MS/MS Method for the Simultaneous Determination of Sofosbuvir and Velpatasvir in Human Plasma-Application to a Pharmacokinetic Study in Egyptian Volunteers. *J. Chromatogr. B: Anal. Technol. Biomed. Life Sci.* **2018**, *1102−1103*, 116−124.

(21) Semreen, M.; Alniss, H.; Mousa, M.; Aboul-Enein, H. Quick and Sensitive UPLC-ESI-MS/MS Method for Simultaneous Estimation of Sofosbuvir and Its Metabolite in Human Plasma. *Molecules* **2019**, *24*, 1302.

(22) Rezk, M. R.; Basalious, E. B.; Badr, K. A. Novel Determination of Sofosbuvir and Velpatasvir in Human Plasma by UPLC-MS/MS Method: Application to a Bioequivalence Study. *Biomed. Chromatogr.* **2018**, *32*, No. e4347.

(23) Rezk, M. R.; Monir, H. H.; Marzouk, H. M. Novel Determination of a New Antiviral Combination; Sofosbuvir and Velpatasvir by High Performance Thin Layer Chromatographic Method; Application to Real Human Samples. *Microchem. J.* **2019**, *146*, 828−834.

(24) Moustapha, M. E.; El-Gamal, R. M.; Belal, F. F. Two Novel UPLC Methods Utilizing Two Different Analytical Columns and Different Detection Approaches for the Simultaneous Analysis of Velpatasvir and Sofosbuvir: Application to Their Co-Formulated Tablet. *BMC Chem.* **2019**, *13*, 118.

(25) El-Gamal, R. M.; Abdel-Gawad, S. A.; Belal, F. F.; Moustapha, M. E. Selective and Sensitive Spectrofluorimetric Quantification of Velpatasvir in Presence of Sofosbuvir. Application to Their Co-Formulated Tablet. *RSC Adv.* **2018**, *8*, 32909−32915.

(26) Alqahtani, S. M.; Alamri, M. A.; Alabbas, A.; Alam, P.; Abdel-Gawad, S. A.; Shakeel, F.; Alasmary, F. A. Spectrophotometric and Spectrodensitometric Quantification of a New Antiviral Combination. *J. Planar Chromatogr.–Mod. TLC* **2020**, *33*, 79−87.

(27) Rezk, M. R.; Monir, H. H.; Marzouk, H. M. Spectrophotometric Assessment of the Brand New Antiviral Combination: Sofosbuvir and Velpatasvir in Their Pure Forms and Pharmaceutical Formulation. *Spectrochim. Acta, Part A* **2019**, *213*, 159−166.

(28) Asran, A. M.; Mohamed, M. A.; Ahmed, N.; Banks, C. E.; Allam, N. K. An Innovative Electrochemical Platform for the Sensitive

Determination of the Hepatitis B Inhibitor Entecavir with Ionic Liquid as a Mediator. *J. Mol. Liq.* **2020**, *302*, 112498.
(29) Mohamed, M. A.; El-Gendy, D. M.; Ahmed, N.; Banks, C. E.; Allam, N. K. 3D Spongy Graphene-Modified Screen-Printed Sensors for the Voltammetric Determination of the Narcotic Drug Codeine. *Biosens. Bioelectron.* **2018**, *101*, 90−95.
(30) Abdullah, I. H.; Ahmed, N.; Mohamed, M. A.; Ragab, F. M. A.; Abdel-Wareth, M. T. A.; Allam, N. K. An Engineered Nanocomposite for Sensitive and Selective Detection of Mercury in Environmental Water Samples. *Anal. Methods* **2018**, *10*, 2526−2535.
(31) Abbas, W. A.; Ramadan, M.; Faid, A. Y.; Abdellah, A. M.; Ouf, A.; Moustafa, N.; Allam, N. K. Photoactive Catalysts for Effective Water Microbial Purification: Morphology-Activity Relationship. *Environ. Nanotechnol. Monit. Manag.* **2018**, *10*, 87−93.
(32) Mohamed, M. A.; Yehia, A. M.; Banks, C. E.; Allam, N. K. Novel MWCNTs/Graphene Oxide/Pyrogallol Composite with Enhanced Sensitivity for Biosensing Applications. *Biosens. Bioelectron.* **2017**, *89*, 1034−1041.
(33) Saleh, M. A.; Taha, M. M.; Mohamed, M. A.; Allam, N. K. A Novel and Ultrasensitive Electrochemical Biosensorbased on MnO_2-V_2O_5 Nanorods for the Detection of the Antiplatelet Prodrug Agent Cilostazol in Pharmaceutical Formulations. *Microchem. J.* **2021**, *164*, 105946.
(34) El-Wekil, M. M.; Mahmoud, A. M.; Marzouk, A. A.; Alkahtani, S. A.; Ali, R. A Novel Molecularly Imprinted Sensing Platform Based on MWCNTs/AuNPs Decorated 3D Starfish like Hollow Nickel Skeleton as a Highly Conductive Nanocomposite for Selective and Ultrasensitive Analysis of a Novel Pan-Genotypic Inhibitor Velpatasvir in Body Fluids. *J. Mol. Liq.* **2018**, *271*, 105−111.
(35) Zhang, L.; Wang, J.; Du, T.; Zhang, W.; Zhu, W.; Yang, C.; Yue, T.; Sun, J.; Li, T.; Wang, J. NH_2-MIL-53(Al) Metal-Organic Framework as the Smart Platform for Simultaneous High-Performance Detection and Removal of Hg^{2+}. *Inorg. Chem.* **2019**, *58*, 12573−12581.
(36) Shahat, A.; Elsalam, S. A.; Herrero-Martínez, J. M.; Simó-Alfonso, E. F.; Ramis-Ramos, G. Optical Recognition and Removal of Hg(II) Using a New Self-Chemosensor Based on a Modified Amino-Functionalized Al-MOF. *Sens. Actuators, B* **2017**, *253*, 164−172.
(37) Mahmoud, A. M.; El-Wekil, M. M.; Mahnashi, M. H.; Ali, M. F. B.; Alkahtani, S. A. Modification of N,S Co-Doped Graphene Quantum Dots with p-Aminothiophenol-Functionalized Gold Nanoparticles for Molecular Imprint-Based Voltammetric Determination of the Antiviral Drug Sofosbuvir. *Microchim. Acta* **2019**, *186*, 617.
(38) El-Wekil, M. M.; Mahmoud, A. M.; Alkahtani, S. A.; Marzouk, A. A.; Ali, R. A Facile Synthesis of 3D $NiFe_2O_4$ Nanospheres Anchored on a Novel Ionic Liquid Modified Reduced Graphene Oxide for Electrochemical Sensing of Ledipasvir: Application to Human Pharmacokinetic Study. *Biosens. Bioelectron.* **2018**, *109*, 164−170.
(39) Samui, A.; Sahu, S. K. One-Pot Synthesis of Microporous Nanoscale Metal Organic Frameworks Conjugated with Laccase as a Promising Biocatalyst. *New J. Chem.* **2018**, *42*, 4192−4200.
(40) Cheng, X.; Zhang, A.; Hou, K.; Liu, M.; Wang, Y.; Song, C.; Zhang, G.; Guo, X. Size- and Morphology-Controlled NH2-MIL-53(Al) Prepared in DMF-Water Mixed Solvents. *Dalton Trans.* **2013**, *42*, 13698−13705.
(41) Sánchez-Sánchez, M.; Getachew, N.; Díaz, K.; Díaz-García, M.; Chebude, Y.; Díaz, I. Synthesis of Metal-Organic Frameworks in Water at Room Temperature: Salts as Linker Sources. *Green Chem.* **2015**, *17*, 1500−1509.
(42) Zhang, L.; Hu, Y. H. A Systematic Investigation of Decomposition of Nano $Zn_4O(C_8H_4O_4)_3$ Metal-Organic Framework. *J. Phys. Chem. C* **2010**, *114*, 2566−2572.
(43) Chang, L.; Li, J.; Duan, X.; Liu, W. Porous Carbon Derived from Metal-Organic Framework (MOF) for Capacitive Deionization Electrode. *Electrochim. Acta* **2015**, *176*, 956−964.
(44) Zhang, W.; Wu, Z.-Y.; Jiang, H.-L.; Yu, S.-H. Nanowire-Directed Templating Synthesis of Metal-Organic Framework Nanofibers and Their Derived Porous Doped Carbon Nanofibers for Enhanced Electrocatalysis. *J. Am. Chem. Soc.* **2014**, *136*, 14385−14388.
(45) Liu, R.-L.; Ji, W.-J.; He, T.; Zhang, Z.-Q.; Zhang, J.; Dang, F.-Q. Fabrication of Nitrogen-Doped Hierarchically Porous Carbons through a Hybrid Dual-Template Route for CO_2 Capture and Haemoperfusion. *Carbon* **2014**, *76*, 84−95.
(46) Lu, T.; Zhang, L.; Sun, M.; Deng, D.; Su, Y.; Lv, Y. Amino-Functionalized Metal-Organic Frameworks Nanoplates-Based Energy Transfer Probe for Highly Selective Fluorescence Detection of Free Chlorine. *Anal. Chem.* **2016**, *88*, 3413−3420.
(47) Ahmadi Feijani, E.; Tavasoli, A.; Mahdavi, H. Improving Gas Separation Performance of Poly(Vinylidene Fluoride) Based Mixed Matrix Membranes Containing Metal-Organic Frameworks by Chemical Modification. *Ind. Eng. Chem. Res.* **2015**, *54*, 12124−12134.
(48) Compton, R. G.; Banks, C. E. Cyclic Voltammetry at Macroelectrodes. *Understanding Voltammetry*; World Scientific, 2007; pp 107−151.
(49) Ziyatdinova, G.; Ziganshina, E.; Budnikov, H. Electrochemical Reduction and Quantification of Menadione in Sodium Dodecyl Sulfate Micellar Media. *J. Solid State Electrochem.* **2013**, *17*, 2679−2685.
(50) Karimi-Maleh, H.; Tahernejad-Javazmi, F.; Ensafi, A. A.; Moradi, R.; Mallakpour, S.; Beitollahi, H. A High Sensitive Biosensor Based on FePt/CNTs Nanocomposite/N-(4-Hydroxyphenyl)-3,5-Dinitrobenzamide Modified Carbon Paste Electrode for Simultaneous Determination of Glutathione and Piroxicam. *Biosens. Bioelectron.* **2014**, *60*, 1−7.
(51) Bali Prasad, B.; Jauhari, D.; Prasad Tiwari, M. A Dual-Template Imprinted Polymer-Modified Carbon Ceramic Electrode for Ultra Trace Simultaneous Analysis of Ascorbic Acid and Dopamine. *Biosens. Bioelectron.* **2013**, *50*, 19−27.
(52) Pan, T.-M.; Mondal, S. Structural Properties and Sensing Characteristics of Sensing Materials. *Comprehensive Materials Processing*; Elsevier, 2014; Vol. *13*, pp 179−203.

https://doi.org/10.1021/acsomega.1c04525
ACS Omega 2021, 6, 26791−26798